



Kaan Orhan, Mert Ocak, and Burak Bilecenoglu

19.1 Micro-computed Tomography (Micro-CT)

Just like tomography, micro-computed tomography (micro-CT) has the ability to create cross-sectional images of a physical object by making use of X-rays. Cross-sectional images created this way are then processed by relevant software in the computer environment, and a three-dimensional model of the scanned object is hence created in the digital environment. Since the pixels forming the 2D cross-sectional images obtained by micro-tomography are in terms of micro- (μ) units, scientific and processable information on internal structures and geometries of tiny objects or appropriately sized pieces of larger objects can be attained. Research on the use of micro-CT and 3D printer technologies for medical and industrial prototyping processes are becoming ever widespread both in our country and throughout the world. Processing of CT or micro-CT scanning data of a biological structure and subsequent modeling of its three-dimensional model in the digital environment create its own application areas in numerous fields. Having the ability to produce structures by using 3D printers, such as cranial models, skeletal models, bones, organs, etc. to be utilized as educational materials in medical faculties or life sciences departments, results in benefits such as more efficient training regarding the field of education. Another application is the modeling and consequent 3D printing of the body part that is to undertake surgery prior to the surgical operation, which allows attaining more efficient results both for patients and surgeons by shortening the duration of surgery and allowing the surgeon to work with a material similar to the patient's own.

K. Orhan (✉)

Department of Dentomaxillofacial Radiology, Ankara University, Faculty of Dentistry, Ankara, Turkey

M. Ocak

Hacettepe University, Faculty of Medicine, Department of Anatomy, Ankara, Turkey

B. Bilecenoglu

Ankara University, Faculty of Dentistry, Department of Anatomy, Ankara, Turkey

Hounsfield created the very first full-body computed tomography device back in 1975, and Hounsfield and Cormack received the Nobel Prize for physiology and medicine with this device in 1979. Main components of the micro-tomography device are the X-ray tube, a computer-driven step motor that intermittently rotates the sample mounted on its body, an image intensifier which focuses the X-rays in the medium onto the camera sensor, a CCD camera which converts X-rays received into image data, an image collector, and a computer that controls all these components. Better spatial resolution is attained by 5–10 μm^3 voxel size scan provided by micro-computerized tomography, compared to 1 mm^3 voxel size scan provided by computerized tomography. This makes viewing areas 1,000,000 times smaller than that could be viewed by computerized tomography possible, which in turn allows conducting more detailed investigations. This was regarded as a revolutionary development [1, 2] (Fig. 19.1).

Micro-CT scanners are mostly utilized in academic and industrial research laboratories. Micro-CT scanners are used in such institutions usually for the examination of mineralized tissues such as the teeth and bones, ceramics, polymers, and biomaterials. Different fields of views (FOV) could be selected by micro-CT devices relevant to the dimensions of the area to be examined, and hence, higher-resolution images can be obtained by working on smaller areas. In vitro and in vivo micro-CT devices are currently available, and varying FOV ratios applied in these devices determine the area to be examined and the resolution to be attained [3, 4]. Similar to the cone beam computed tomography devices, micro-CT systems utilize microfocal X-ray sources and high-resolution detectors to create 3D reconstructions of the samples. Main components of the micro-tomography device are the X-ray tube, a computer-driven step motor that intermittently rotates the sample mounted on its body, an image intensifier which focuses the X-rays present in the environment onto the camera sensor, a CCD camera which converts X-rays received into image data, an image collector, and a computer that controls all these components [5].

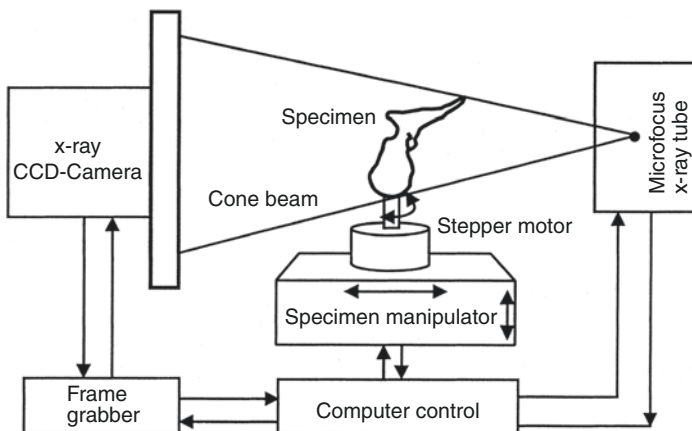


Fig. 19.1 Schematic diagram of micro-computed tomography workflow

19.2 Fundamentals of Micro-computed Tomography (Micro-CT)

From a technical point of view, micro-computed tomography (micro-CT) indeed is a CBCT technique which utilizes geometrically cone-shaped beams for reconstruction and back-projection processes. In contrast to the fan-shaped beams and multiple rotations used in spiral and conventional CT techniques, this technique utilizes a conical X-ray beam, whereas the scanning process is performed by a rotation of 180° or 360° around the field to be scanned, just as it is for CBCT. Having the same operating principle with CBCT, computerized micro-tomography's operating principle is a micro-focus tube that generates X-rays and high-resolution detectors that rotate around the object that is to be scanned, in order to obtain a three-dimensional image of the object. Digital data created by these projections are then converted into images through certain reconstruction algorithms [6–11]. These images can be uploaded to computer environment and if necessary can be modeled in 3D, by using relevant software [1, 2, 9]. These images can be uploaded to computer environment, and if necessary, 3D analyses can be conducted by using relevant software [9]. Micro-tomography (micro-CT) can be used for volumetric and surface measurements of bone tissue whose images were scanned beforehand through cone beam computed tomography. These images are considered equivalent since both CBCT and micro-CT operate on the same working principles. Research cases that evaluate CBCT images by micro-CT software can be found in literature. Reliability of this technique was speculated by researchers. However, they did not come up with a statistically significant difference resulting from analyses of images obtained by two separate devices through micro-CT software [12–15] (Fig. 19.2).

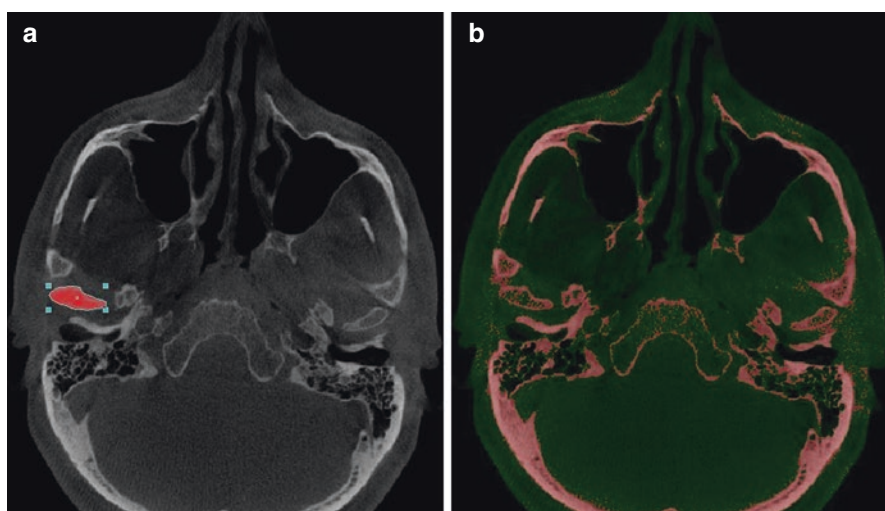


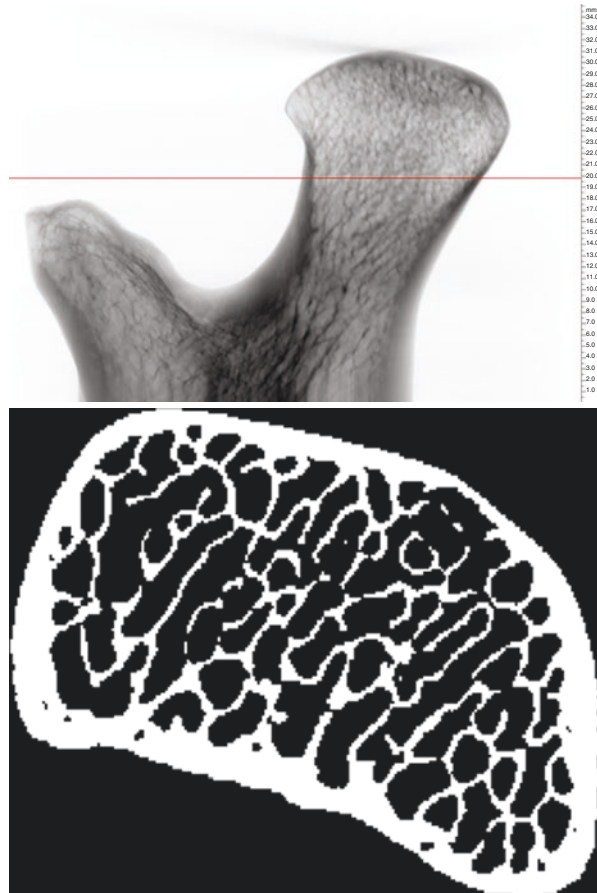
Fig. 19.2 (a) ROI selection for mandibular condyle boundaries for quantitative bone measurements. (b) The filtered mask of the CBCT image for bone analysis using micro-CT software

19.3 Analysis of Bone Micro-architecture via Micro-computed Tomography (Micro-CT)

The term “bone quality” is commonly used in literature to describe the structural formation and boundaries of the bones. The bone quality is definitely associated with trabecular bone structure. Trabecular bone is the primary anatomical and functional structure of the cancellous bone [16] (Fig. 19.3).

Histomorphometric analyses are destructive, long-term, and costly methods. It is impossible to reuse the same sample for another measurement. Moreover, various artifacts might occur due to slices used for sample preparation, which makes an accurate interpretation of analyses even more tedious. Due to these disadvantages, three-dimensional micro-tomography techniques have been put into use as nondestructive, rapid, and reliable methods for analyzing micro-architecture of the cortical and trabecular bones [17].

Fig. 19.3 Black and white binarization of ROI after global thresholding procedure



This can be achieved via the use of certain parameters such as trabecular thickness (Tb.Th), trabeculation number (Tb.N), trabecular separation (Tb.Sp), bone volume (BV), total tissue volume (TV), trabecular bone ratio (BV/TV), structural model index (SMI) that demonstrates numeric features of trabeculation in 3D, trabecular bone junctions, number of trabecular nodes in each tissue volume (N.Nd/TV), and bone density determined with respect to hydroxyapatite count [18].

Tissue volume (TV), bone volume (BV), percent bone volume (BV/TV) are major parameters that can be calculated in Micro-CT evaluations. BV/TV refers to the total amount of bone present in relation to the analyzed bone volume. It is a parameter widely used in pathologies that alter bone turnover as it reflects perfectly bone gain/loss. It indicates the fraction of a given volume of interest occupied by mineralized tissue.

- Bone surface (BS), the surface area of all the solid objects (bone tissue) within the tissue volume (TV), measured in 3D marching cube method. Bone surface (BS) of the sample and bone surface density (BS/BV) is the relationship between the overall trabecular bone surface and the bone volume of the mineralized bone. But a trabecular bone region does not, for example, extend into or beyond the boundary of the object—such as the cortical boundary of a bone sample. The meaningfulness of measured percent volume depends on the criteria applied in selecting the volume of interest. If the ROI or VOI boundaries are loosely drawn in the surrounding space around an object, for instance, then % object volume has no meaning [18].
- Bone-specific surface (BS/TV) analyzes the relation between the trabecular bone surface and the mineralized bone. In a 3D image, it directly measures distance in space.
- Trabecular thickness determines bone fill as well as the mean thickness of the osseous structures. With 3D image analysis by micro-CT, a true 3D thickness can be measured which is model independent.
- Trabecular separation (Tb.Sp) detects marrow spaces and thus should be correlated to BV/TV: The more BV/TV, the less Tb.Sp. This parameter determines inverse bone density. Histomorphometrists typically measure a single mean value of bone Tb.Th from a trabecular bone site. However a trabecular bone volume—or any complex biphasic object region—can also be characterized by a distribution of thicknesses. Micro-CT outputs a histogram of thickness (and separation also) with an interval of two pixels. Thickness distribution is a powerful method for characterizing the shape of a complex structure [19].
- The trabecular number implies the number of times a trabecular structure is crossed per unit length in a randomly selected way.
- Bone quality is determined by direct nonmetric parameters. Trabecular pattern factor (Tb.Pf) describes quantitatively trabecular connectivity. It is an inverse connectivity index. Therefore, the concavity of the trabecular surfaces implies connectivity, whereas convexity means isolated and misconnected structures. This is an inverse index of connectivity, which was developed and defined by Hahn et al. [16] for application to the trabecular bone. Tb.Pf is calculated in 3D, by comparing volume and surface of binarized solid before and after a single voxel image dilation [16].

- The structural model index determines the relative presence of either plate-like or rod-like trabeculae. It is defined in a range of 0–3, where closer to 0 corresponds to an ideal plate and 3 to an ideal cylinder. Normally, plate-like trabeculae are associated with a higher osseous stiffness. SMI involves a measurement of surface convexity. This parameter is of importance in osteoporotic degradation of the trabecular bone which is characterized by a transition from plate-like to rod-like architecture. An ideal plate, cylinder, and sphere have SMI values of 0, 3, and 4, respectively [20].
- The fractal dimension (FD) fractal analysis is a statistical texture analysis that is based on fractal mathematics for describing complex shapes and structural patterns. It is expressed numerically as “fractal dimension” (FD), which measures self-similarity and indicates a figure’s complexity. For the 3D calculation of FD, the volume is divided into an array of equal cubes, and the number of cubes containing part of the object surface is counted.
- Bone mineral density compares between the attenuation coefficients of two hydroxyapatite patterns of known density (250 and 750 mg/cm³). This is an area of density and not a true volume density as it has a dependency on bone size [21, 22] (Figs. 19.4 and 19.5).

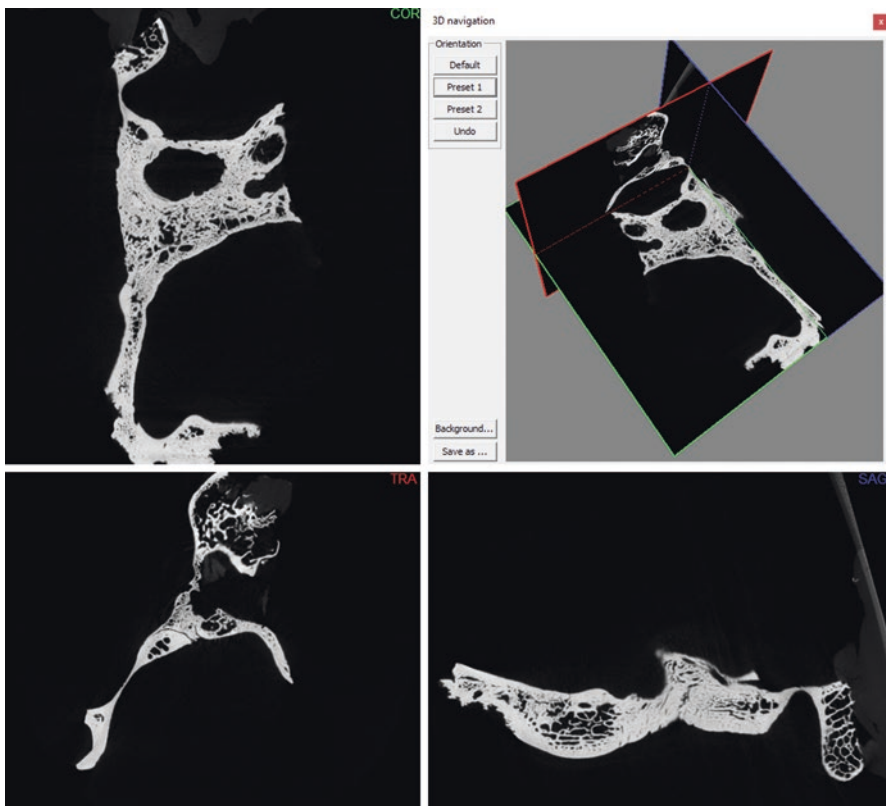


Fig. 19.4 Images of axial, transverse, and coronal sections of the temporal bone and fossa mandibularis

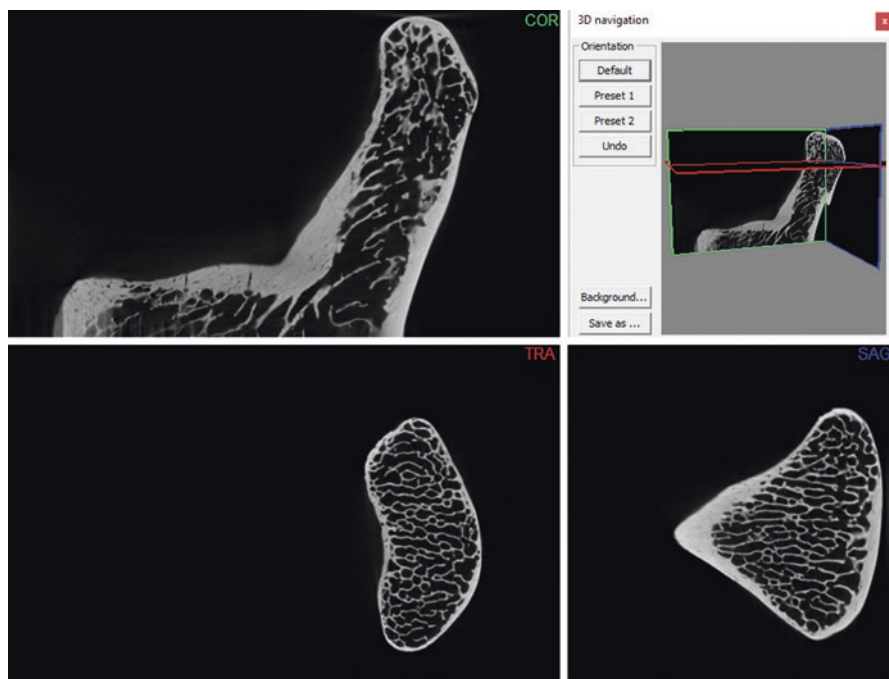


Fig. 19.5 Images of axial, transverse and coronal sections of the mandibular condyle

Dessel et al. [15] worked on determining the accuracy of cone beam CT (CBCT) measurement of trabecular bone microstructure in mandibulae, compared to that measured by micro-CT. They hydrostatically scanned eight mandibulae using three different CBCT protocols and consequently scanned with micro-CT. No statistically significant difference was found for the resulting images.

19.4 Micro-computed Tomography (Micro-CT) in TMJ Bone Research

Images are automatically converted to 8-bit axial images through relevant software for TMJ research. Bone components related to joints are identified in axial images, along with the determination of upper and lower limits required for the realization of analyses. ROIs (regions of interest) are selected by determining bone regions in axial images that lie within these limits. Black and white pixel ranges are determined by setting semiautomatic histogram settings, and global thresholding procedure is applied for realization of automatic analyses within these reference ranges. To make things clear, the gray image that belongs to ROIs within the corresponding range is pixelated as black and white dots. Total tissue volume, total bone volume, bone surface area, percentage rate of bone tissue, and aforementioned detailed trabeculae structure analyses can be measured along the selected ROI regions by the help of relevant software.

The percentage rate of bone tissue reflects the total bone amount that is associated with the analyzed bone volume. It is a parameter used for cases with bone replacement, and it perfectly reflects bone gain and bone loss. It shows the fraction of the volume occupied by the mineralized tissue. Bone surface indicates the total trabecular bone surface [9] (Figs. 19.6, 19.7 and 19.8).

Mulder et al. [23] examined the structure, mineralization, and trabecular bone development of pig condyle by using micro-computed tomography. They found out that the remodeling patterns of anterior and posterior mandibular condyle were

Fig. 19.6 3D reconstruction of the temporal bone

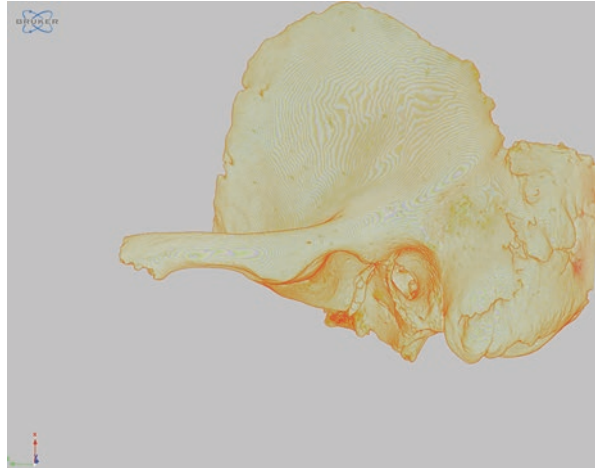


Fig. 19.7 3D reconstruction of the mandibular condyle from coronal view



Fig. 19.8 3D reconstruction of the mandibular condyle from sagittal view



different from each other and that the condyle grew more in posterior direction, as a result of this study. They also demonstrated that the trabecular bone volume and thickness were higher in the corpus and that the mineralization value was the same for both the anterior and posterior of the condyle, with the corpus having a higher mineralization value.

Suomalainen et al. [10] scanned the TMJ samples obtained from postsurgical biopsy materials by using micro-CT. They declared that the micro-CT device visualized bone anatomical structures in a precise manner, making it a reliable tool—for instance—with respect to planning of joint prosthesis and treatment, as a result of this study. They also concluded that the device was pretty convenient to be used for diagnosing dental infections.

Kim et al. [24] performed micro-CT analyses in healthy mandibular condyle obtained from nine male cadavers. They succeeded in both imaging the condyle's bone micro-architecture thoroughly and conducting clinically important analyses by creating 3D models of these structures.

In their research conducted with mice, Zhang et al. [25] investigated the effect of platelet-rich plasma treatment (PRP) for bone replacement resulting from loss of the teeth. They defined condylar cartilage and related regions of subcondylar region as their ROI and utilized a total of five consecutive images of ROI for three-dimensional reconstruction and analyses during their research. By analyzing these images, they calculated total volume (BV), trabecular number (Tb.N), trabecular separation (Tb.Sp.), and trabecular bone volume (Tb.Th) per trabecular thickness.

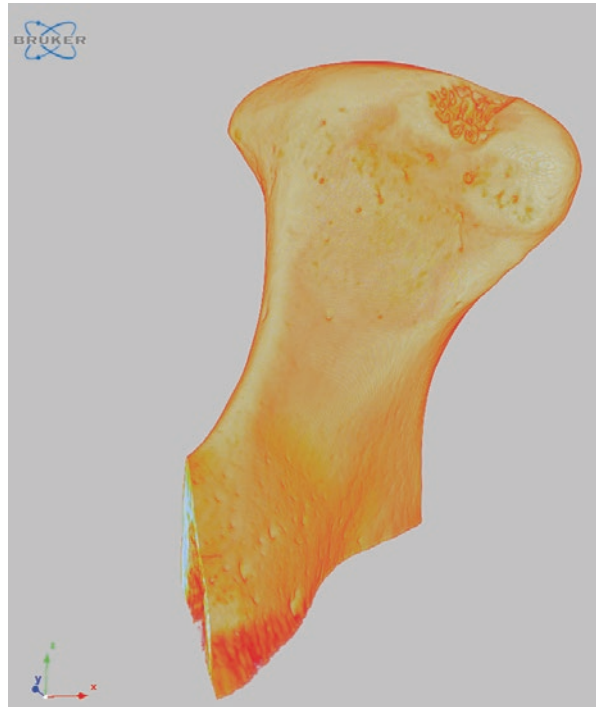
Kaur et al. [26], in their study conducted with 54 Sprague–Dawley rats for studying bone structural parameters, calculated the bone volume to tissue volume ratio (bone volume fraction), trabecular thickness, trabecular number, trabecular separation, and bone mineral density. They compared other imaging techniques through these values by taking micro-CT values as the gold standard.

In another study investigating the effects of chewing muscle atrophy on TMJ, Kün-Darbois et al. [27] used micro-CT to calculate the amount of resorption in alveolar bone and mandibular condyle in adult mice that had been subjected to botox application on the masseter muscle.

Variants of these analyses that can easily be conducted by using micro-CT software can also be performed by using numerous 3D software. Either micro-CT scan images or images obtained from other imaging techniques that work on similar principles can be processed through the software. Gomes et al. [28] scanned 169 TMJ condyles that exhibited osteoarthritis variations (69 subjects with long-term TMJ osteoarthritis (OA), 15 subjects at initial diagnosis of OA, and 7 healthy controls) with CBCT. They consequently created three-dimensional surface models of these condyles through using a special software. As a result of their study, they identified a preliminary diagnostic index for 3D osteoarthritic changes. Cevidanes et al. [29] also conducted a research in order to evaluate the registry of 3D models obtained from CBCT images taken pre- and post-orthognathic surgeries for the assessment of mandibular anatomy and position of mandibulae. CBCT scans were obtained during pre- and post-orthognathic surgery for ten patients that have various malocclusions. These pre- and postsurgery images were reconstructed in 3D and superimposed on each other, and the regions where changes were observed were shown in different colors. Cevidanes et al. [30] reused this method of superimposing 3D models on each other, in order to observe growth-related maxillofacial changes. Researchers obtained pre- and posttreatment CBCT images of three Class III malocclusion patients that are to be orthopedically treated with miniplates. They observed the course of treatment for these patients throughout 1 year, creating 18 pieces of 3D virtual surface models, and then superimposed these images on one another, coloring the growth-related changes. Numerous studies based on 3D reconstruction of bone micro-architecture such as these can be found in literature [31–33]. Three-dimensional (3D) imaging techniques can provide valuable information for clinicians and researchers. However, considering that we recently moved from traditional two-dimensional (2D) cephalometric analyses to novel 3D techniques, we should thus be comparing data obtained by 2D and 3D methods. Regarding a study based on this problem [34], it was proven that CBCT images could effectively be used along with 3D modeling methods.

Micro-CT is used not only in adult TMJ imaging but also in experimental growth studies. In a study conducted with Sprague–Dawley rats that were exposed to effects of various hormones, Khan et al. [35] observed the growth of mandibulae, and they scanned the rats' mandibulae after dissecting them when they were 21 days old. They consequently calculated the bone volume and bone surface area of corresponding mandibulae as well as their bone mineral densities (Figs. 19.9, 19.10, and 19.11).

Fig. 19.9 3D reconstruction of osteoarthritis mandibular condyle



19.5 Micro-computed Tomography and TMJ Bone Histopathology

The bone is a highly mineralized and multifunctional tissue, which plays the roles in mechanical support and protection, mineral homeostasis, and hematopoiesis. In recent years, it has become clear that the bone also serves an essential endocrine function. To achieve these functional goals, the bone is organized hierarchically, from nanometer- to millimeter-sized structures. This contributes not only to its mechanical role in support and movement of the body but also to its other functions. At the nanostructural level, the bone is composed of organic and mineral components, mainly consisting of a matrix of cross-linked type I collagen mineralized with nanocrystalline, carbonated apatite. Due to its high mineral content, the bone tissue is extremely resilient, but its organic part also provides a certain degree of flexibility and elasticity improving its behavior under mechanical forces [36, 37].

The “quality” of the bone, as well as its quantity, contributes to the biomechanical performance of the skeleton and encompasses aspects of both macromolecular composition and micro-architectural arrangement [38].

Bone histomorphometry is an essential tool for understanding tissue-level mechanisms of bone physiology and assessing the mechanisms by which bone diseases occur, the mechanisms by which therapeutic agents affect the skeleton, and the

Fig. 19.10 3D reconstruction of normal mandibular condyle

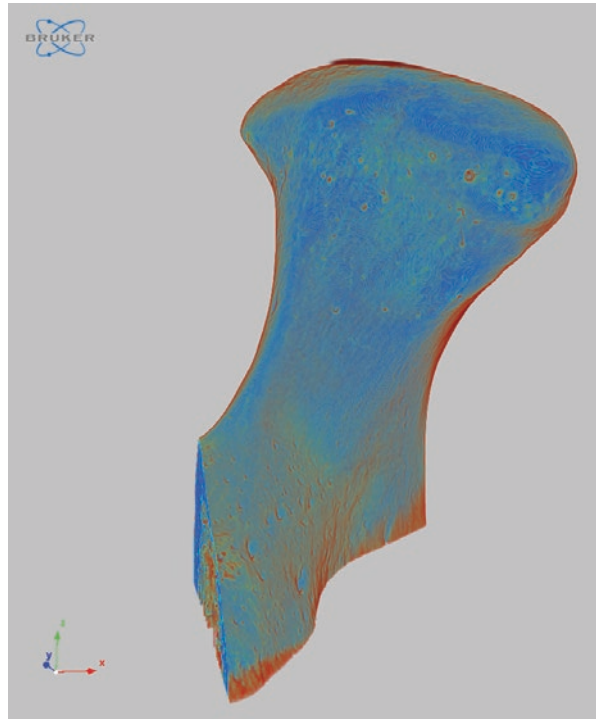
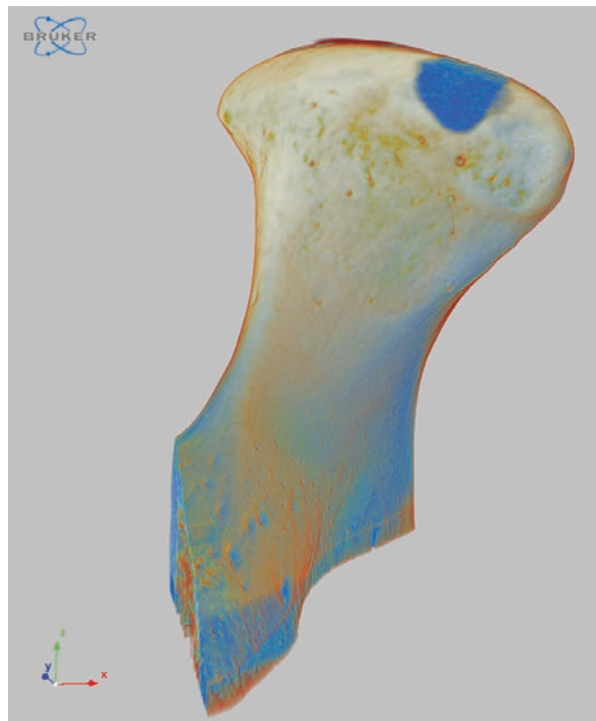


Fig. 19.11 3D registration of normal and osteoarthritic mandibular condyle



skeletal safety of therapeutic agents. It is the gold standard for tissue-level bone activity. It can yield a wealth of information about the bone structure, bone formation, bone resorption, bone mineralization, as well as bone modeling and remodeling activity [39].

Cancellous bone volume can be measured on histologic sections. A more detailed evaluation of trabecular architecture, such as thickness, number, and separation, can be calculated from the primary measures of bone area and surface. Cortical geometry, such as bone area and periosteal and endosteal perimeters can be directly measured [37].

Discriminating between woven and lamellar bone tissue can be valuable for determining whether the bone formation is occurring in a normal fashion. Evaluating lamellar and woven bone is accomplished using polarized light microscopy on unstained sections, although some stains allow collagen orientation to be visualized. In pathologic conditions such as Paget's disease of the bone, the presence of woven bone provides key diagnostic criteria. Lamellar bone, viewed under polarized light, can be assessed in more detail to elucidate features such as the number of lamellae within a given basic multicellular unit (BMU), the thickness of lamellae, or the type of lamellar organization (alternating or homogeneous) [37].

Using stains for osteoid, the examination of mineralized versus nonmineralized bone can provide information about changes in the mineralization process. Analysis of osteoid involves measuring the extent of the bone surface covered by osteoid (and then normalizing it by the total bone surface examined) and either the width or volume of osteoid. Although called osteoid volume in the literature, this is actually an area (given that it is a 2D assessment). If osteoid width is normal, increased osteoid surface is indicative of higher bone formation. Increased width of osteoid is indicative of a mineralization defect [37].

The extent of surfaces covered with osteoblasts and osteoclasts provides a primary index of how bone formation and/or resorption is altered under various conditions. Osteoblasts can be identified using morphological characteristics on sections stained with Goldner's trichrome, von Kossa and McNeal's, or even hematoxylin and eosin. Primary outcomes related to osteoblasts include osteoblast surface and their number, both typically normalized to bone surface. The most commonly employed technique for assessing activity of resorption is to measure eroded (or resorption) surfaces or erosion depth. A variable related to erosion depth from previous remodeling activity is average wall width (W.Wi), a measure of the amount of the bone formed at a given BMU. The balance between W.Wi and erosion depth determines BMU balance [37].

Although osteoblast function can be inferred through measures of osteoid, the most commonly used method is the assessment of fluorochrome labels (dynamic histomorphometry), because it allows the calculation of rates of modeling and remodeling. Mineralizing surface is reported per unit bone surface (MS/BS, %) by dividing the mineralizing surface by the total bone surface measured. MS/BS is often considered an index of osteoblast activity such that interventions that impact osteoblast proliferation and/or differentiation would be expected to change MS/BS [37].

The mineral apposition rate (MAR) is a commonly used parameter for the characterization of bone formation and is often determined to test for experimental effects on the cortical bone.

During histomorphometric analysis, different staining methods can be used which highlight certain features. During histomorphometric analysis, different staining methods can be used which highlight certain features. Toluidine blue is used to identify cavities under polarized light by looking at the presence of cutoff collagen fibers (disruption of the lamellar system) at the edge of the cavity. The polarized light allows visualization of the orientation of collagen lamellae along the mineralized bone surface. The identification of scalloped surfaces can, however, be subjective. Tartrate-resistant acid phosphatase can be used to mark active osteoclasts and thus “active” cavities. Von Kossa/van Gieson staining allows discriminating osteoid from mineralized bone [37, 38].

Before histomorphometric analyses take place, study specimens are subjected to a complex preparation protocol, from sample collection to microscopical observation of the prepared slide: sample collection, fixation and dehydration, infiltration and embedding, orientation/plane of section, and staining.

Using the histologic sections for quantification, the paraffin-embedded sections can distort and shrink up to 15%. This can make a big difference in histologic measurements and potentially obscure real differences between groups. Another limitation of paraffin embedding is that decalcification is usually incomplete. Thus, tissue sectioning is very challenging, resulting in suboptimal sections for analysis. Also, measurement variance associated with bone histomorphometry arises from some factors including intraobserver, interobserver, intermethod, and sample variation. Observer variation is mainly due to the subjective criteria used for identification of features such as osteoid seams, bone structural units, and resorption cavities. The protocol complexity, costs, required time, and high level of expertise and training are limitations of bone histomorphometry. It is also a two-dimensional and invasive technique [37, 38, 40, 41].

More recently micro-computed tomography appeared. It is capable of forming both 2D and 3D images with applications in bone formation quantification, as well as in bone modeling in bone grafts. It is also fast and allows nondestructive analysis without a specific preparation protocol.

The excellent reproducibility and accuracy of micro-CT measurements of bone morphology have been established in several studies [42, 43]. The accuracy of micro-CT morphology measurements has been evaluated by comparing them with traditional measures from 2D histomorphometry both in animal and in human specimens [42, 44, 45]. These studies show that 2D and 3D morphologic measurements by micro-CT generally are highly correlated with those from 2D histomorphometry [46].

Ex vivo micro-CT scanners typically produce scans with pixel sizes in the range of 1–30 μm . This provides sufficient resolution to accurately detect individual trabecular structures in small rodents, such as rats and mice, as well as in larger species. Higher-resolution scans, on a nanometer scale, can be obtained with nano-CT and synchrotron-CT machines [37].

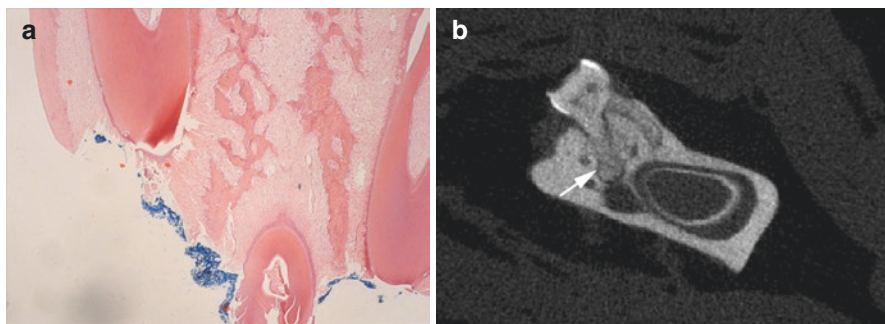


Fig. 19.12 (a) Histopathological image of a rat mandible. (b) Corresponding micro-CT slice showing destruction of the mandibular bone (arrow)

There are numerous advantages to using micro-CT for assessment of bone mass and morphology in excised specimens: (1) It allows for direct 3D measurement of trabecular morphology, such as trabecular thickness and separation, rather than inferring these values based on 2D stereologic models, as is done with standard histologic evaluations; (2) compared with 2D histology, a significantly larger volume of interest is analyzed; (3) measurements can be performed with a much faster throughput than typical histologic analyses of histomorphometric parameters using undecalcified bone specimens; and (4) assessment of bone morphology by micro-CT scanning is nondestructive; thus samples can be used subsequently for other assays, such as histology or mechanical testing [43, 47].

Micro-CT presents advantages over histomorphometry, but only the latter one can make cellular-level observation [48]. The additional value of micro-CT imaging is that it allows to provide details on the morphology of the cancellous network (avoiding assumptions of trabecular morphology) and more detailed data on cortical bone geometry. It is, therefore, beneficial to use a combination of both histomorphometry and micro-CT to increase the obtained information (Fig. 19.12).

Acknowledgments The authors would like to thank Dr. Umut Aksoy for the preparation of micro-computed tomography and TMJ bone histopathology section and providing histopathology and corresponding rat mandibular micro-CT image.

All specimens in this chapter were scanned with Skyscan 1275 (Skyscan, Kontich, Belgium) which were taken from the Ankara University Research Fund (Project No:17A0234001).

References

1. Feldkamp LA, Goldstein SA, Parfitt AM, Jesion G, Kleerekoper M. The direct examination of three-dimensional bone architecture in vitro by computed tomography. *J Bone Miner Res.* 1989;4(1):3–11.
2. Kuhn J, Goldstein S, Feldkamp L, Goulet R, Jesion G. Evaluation of a microcomputed tomography system to study trabecular bone structure. *J Orthop Res.* 1990;8(6):833–42.

3. Guldberg RE, Ballock RT, Boyan BD, Duvall CL, Lin AS, Nagaraja S, Oest M, Phillips J, Porter BD, Robertson G, Taylor WR. Analyzing bone, blood vessels, and biomaterials with microcomputed tomography. *IEEE Eng Med Biol Mag.* 2003;22(5):77–83.
4. Guldberg RE, Lin AS, Coleman R, Robertson G, Duvall C. Microcomputed tomography imaging of skeletal development and growth. *Birth Defects Res C Embryo Today.* 2004;72(3):250–9.
5. Rhodes JS, Ford TR, Lynch JA, Liepins PJ, Curtis RV. Micro-computed tomography: a new tool for experimental endodontology. *Int Endod J.* 1999;32(3):165–70.
6. Arai Y, Tammisalo E, Iwai K, Hashimoto K, Shinoda K. Development of a compact computed tomographic apparatus for dental use. *Practice.* 1999;12:15.
7. Araki K, Maki K, Seki K, Sakamaki K, Harata Y, Sakaino R, et al. Characteristics of a newly developed dentomaxillofacial X-ray cone beam CT scanner (CB MercuRay™): system configuration and physical properties. *Dentomaxillofac Radiol.* 2014;33(1):51–9.
8. Mozzo P, Procacci C, Tacconi A, Martini PT, Andreis IB. A new volumetric CT machine for dental imaging based on the cone-beam technique: preliminary results. *Eur Radiol.* 1998;8(9):1558–64.
9. Orhan K, Ocak M. Use of micro-computerized tomography (micro-CT) in dentistry (Diş hekimliğinde mikro-bilgisayarlı tomografi (Mikro-BT) kullanımı) (Turkish). In: Yakıncı ME, Polat S, editors. *Ulusal mikro-ct yaz okulu ders notları.* Ankara: 72 Tasarım Ltd; 2016.
10. Suomalainen A, Vehmas T, Kortensniemi M, Robinson S, Peltola J. Accuracy of linear measurements using dental cone beam and conventional multislice computed tomography. *Dentomaxillofac Radiol.* 2014;37(1):10–7.
11. Weber AL. History of head and neck radiology: past, present, and future 1. *Radiology.* 2001;218(1):15–24.
12. Ho J-T, Wu J, Huang H-L, Chen MY, Fuh L-J, Hsu J-T. Trabecular bone structural parameters evaluated using dental cone-beam computed tomography: cellular synthetic bones. *Biomed Eng Online.* 2013;12(1):115.
13. Ordinola-Zapata R, Bramante C, Versiani M, Moldauer B, Topham G, Gutmann J, et al. Comparative accuracy of the Clearing Technique, CBCT and Micro-CT methods in studying the mesial root canal configuration of mandibular first molars. *Int Endod J.* 2017;50(1):90–6.
14. Parsa A, Ibrahim N, Hassan B, Stelt P, Wismeijer D. Bone quality evaluation at dental implant site using multislice CT, micro-CT, and cone beam CT. *Clin Oral Implants Res.* 2015;26(1):e1–7.
15. Van Dessel J, Huang Y, Depypere M, Rubira-Bullen I, Maes F, Jacobs R. A comparative evaluation of cone beam CT and micro-CT on trabecular bone structures in the human mandible. *Dentomaxillofac Radiol.* 2013;42(8):20130145.
16. Hahn M, Vogel M, Pompesius-Kempa M, Delling G. Trabecular bone pattern factor – a new parameter for simple quantification of bone microarchitecture. *Bone.* 1992;13:327–30.
17. Parfitt AM. Bone histomorphometry: proposed system for standardization of nomenclature, symbols, and units. *Calcif Tissue Int.* 1988;42:284–6.
18. Currey JD. The many adaptations of bone. *J Biomech.* 2003;36:1487–95.
19. Odgaard A, Gundersen HJ. Quantification of connectivity cancellous bone, with special emphasis on 3-D reconstructions. *Bone.* 1993;14:173–82.
20. Hildebrand T, Rueggsegger P. Quantification of bone microarchitecture with the structure model index. *Comput Methods Biomech Biomed Engin.* 1997;1:15–23.
21. Southard TE, Southard KA, Krizan KE, Hillis SL, Haller JW, Keller J, et al. Mandibular bone density and fractal dimension in rabbits with induced osteoporosis. *Oral Surg Oral Med Oral Pathol Oral Radiol Endod.* 2000;89:244–9.
22. Tosoni GM, Lurie AG, Cowan AE, Burleson JA. Pixel intensity band fractal analyses: detecting osteoporosis in perimenopausal and postmenopausal women by using digital panoramic images. *Oral Surg Oral Med Oral Pathol Oral Radiol Endod.* 2006;102:235–41.
23. Mulder L, Koolstra JH, Weijs WA, van Eijden TM. Architecture and mineralization of developing trabecular bone in the pig mandibular condyle. *Anat Rec A Discov Mol Cell Evol Biol.* 2005;285(1):659–66.

24. Kim JE, Yi WJ, Heo MS, Lee SS, Choi SC, Huh KH. Three-dimensional evaluation of human jaw bone microarchitecture: correlation between the microarchitectural parameters of cone beam computed tomography and micro-computer tomography. *Oral Surg Oral Med Oral Pathol Oral Radiol.* 2015;120(6):762–70.
25. Zhang YT, Niu J, Wang Z, Liu S, Wu J, Yu B. Repair of osteochondral defects in a rabbit model using bilayer Poly(Lactide-co-Glycolide) scaffolds loaded with autologous platelet-rich plasma. *Med Sci Monit.* 2017;23:5189–201.
26. Kaur H, Uludağ H, Dederich DN, El-Bialy T. Effect of increasing low-intensity pulsed ultrasound and a functional appliance on the mandibular condyle in growing rats. *J Ultrasound Med.* 2017;36(1):109–20.
27. Kün-Darbois JD, Libouban H, Chappard D. Botulinum toxin in masticatory muscles of the adult rat induces bone loss at the condyle and alveolar regions of the mandible associated with a bone proliferation at a muscle enthesis. *Bone.* 2015;77:75–82. <https://doi.org/10.1016/j.bone.2015.03.023>.
28. Gomes LR, Gomes MR, Jung B, Paniagua B, Ruellas AC, Gonçalves JR, et al. Diagnostic index of three-dimensional osteoarthritic changes in temporomandibular joint condylar morphology. *J Med Imaging.* 2015;2(3):034501.
29. Cevidanes LH, Bailey L, Tucker G Jr, Styner M, Mol A, Phillips C, et al. Superimposition of 3D cone-beam CT models of orthognathic surgery patients. *Dentomaxillofac Radiol.* 2005;34(6):369–75.
30. Cevidanes LH, Heymann G, Cornelis MA, DeClerck HJ, Tulloch JC. Superimposition of 3-dimensional cone-beam computed tomography models of growing patients. *Am J Orthod Dentofac Orthop.* 2009;136(1):94–9.
31. Cevidanes LH, L'Tanya JB, Tucker SF, Styner MA, Mol A, Phillips CL, et al. Three-dimensional cone-beam computed tomography for assessment of mandibular changes after orthognathic surgery. *Am J Orthod Dentofac Orthop.* 2007;131(1):44–50.
32. De Clerck H, Nguyen T, De Paula LK, Cevidanes L. Three-dimensional assessment of mandibular and glenoid fossa changes after bone-anchored class III intermaxillary traction. *Am J Orthod Dentofac Orthop.* 2012;142(1):25–31.
33. Goncalves JR, Wolford LM, Cassano DS, Da Porciuncula G, Paniagua B, Cevidanes LH. Temporomandibular joint condylar changes following maxillomandibular advancement and articular disc repositioning. *J Oral Maxillofac Surg.* 2013;71(10):1759.e1–e15.
34. Cevidanes LH, Styner MA, Proffit WR. Image analysis and superimposition of 3-dimensional cone-beam computed tomography models. *Am J Orthod Dentofac Orthop.* 2006;129(5):611–8.
35. Khan I, El-Kadi A, El-Bialy T. Effects of growth hormone and ultrasound on mandibular growth in rats: microCT and toxicity analyses. *Arch Oral Biol.* 2013;58(9):1217–24.
36. Clarke B. Normal bone anatomy and physiology. *Clin J Am Soc Nephrol.* 2003;3(3):131–9.
37. Allen MR, Burr DB. Techniques in histomorphometry. In: *Basic and applied bone biology.* London: Academic Press; 2014. p. 131–48.
38. Aaron JE, Shore PA. Bone histomorphometry. In: *Handbook of histology methods for bone and cartilage.* New York: Humana; 2003. p. 331–51.
39. Erben RG, Glösmann M. Histomorphometry in rodents. In: *Bone research protocols.* New York: Humana; 2012. p. 279–303.
40. Vandeweghe S, Coelho PG, Vanhove C, Wennerberg A, Jimbo R. Utilizing micro-computed tomography to evaluate bone structure surrounding dental implants: a comparison with histomorphometry. *J Biomed Mater Res B Appl Biomater.* 2013;101(7):1259–66.
41. Vedi S, Compston J. Bone histomorphometry. In: *Bone research protocols.* New York: Humana; 2003. p. 283–98.
42. Bouxsein ML, Boyd SK, Christiansen BA, Guldberg RE, Jepsen KJ, Müller R. Guidelines for assessment of bone microstructure in rodents using micro-computed tomography. *J Bone Miner Res.* 2010;25(7):1468–86.
43. Chappard D, Retailleau-Gaborit N, Legrand E, Baslé MF, Audran M. Comparison insight bone measurements by histomorphometry and μ CT. *J Bone Miner Res.* 2005;20(7):1177–84.

44. Bonnet N, Laroche N, Vico L, Dolleans E, Courteix D, Benhamou CL. Assessment of trabecular bone microarchitecture by two different x-ray microcomputed tomographs: a comparative study of the rat distal tibia using Skyscan and Scanco devices. *Med Phys*. 2009;36(4):1286–97.
45. Müller R, Van Campenhout H, Van Damme B, Van Der Perre G, Dequeker J, Hildebrand T, Rügsegger P. Morphometric analysis of human bone biopsies: a quantitative structural comparison of histological sections and micro-computed tomography. *Bone*. 1998;23(1):59–66.
46. Matthew AR, Burr DB. Techniques in histomorphometry. In: *Basic and applied bone biology*. New York: Elsevier; 2014. p. 131–48.
47. Swain MV, Xue J. State of the art of micro-CT applications in dental research. *Int J Oral Sci*. 2009;1(4):177–88.
48. Compston JE. Bone density: BMC, BMD, or corrected BMD? *Bone*. 1995;16:5–7.